EFFECT OF PULSE-HEIGHT SELECTION ON LESION DETECTION PERFORMANCE

F. D. Rollo* and A. G. Schulz

The Johns Hopkins Medical Institutions, Baltimore, Maryland and The Johns Hopkins University Applied Physics Laboratory, Silver Spring, Maryland

It was the purpose of this study to investigate the extent to which window selection affects observer detection of a lesion located within an organ with a particular scatter geometry and activity distribution when a specific collimated detector system is used.

Sanders, Cohen, and Kuhl (*1*) as well as Beck and Harper (*2*) have studied the effect of pulse-height selection in imaging systems in their attempts to establish an optimum window setting for ^{99m}Tc in brain scanning. Sanders et al asked observers to judge image "quality" in a number of scans made with various window settings. Beck's approach involved the use of a statistically based quality factor to establish the test window setting. While both approaches provide useful information, neither method is capable of providing quantitative data on how pulse-height selection affects lesion detectability as a function of lesion size, scatter condition, or radionuclide type.

In the present study a computer program was developed to generate a simulated scan which reflected the overall effect of pulse-height selection on sensitivity (count density), spatial resolution, and contrast. The images of several hundred of these simulated scans were viewed by observers, and the relative threshold of detectability of lesions was measured as a function of window settings for ^{197}Hg as well as for ^{99m}Tc. The results of these observer studies provided data on the quantitative variation in the threshold detection of focal lesions. From these lesion detection performance curves, the optimum window settings based on threshold detection of lesions may be determined.

The simulation method has the advantage of incorporating the total effect of pulse-height selection in the simulated scan while the evaluation technique has the unique feature of including the psychological and physiological factors affecting observers in detecting lesions.

SIMULATION OF SCAN IMAGES

To study the effects of photon-energy selection on the threshold detectability of lesions, it is necessary to provide an accurate and realistic simulation of all features of the scan with particular care to include all effects arising from variations in window setting. The generation of the simulated scan data was based upon the measured spatial response functions of the Magnascanner III collimator detector with a collimator having a 0.625 cm FWHM. The mean number of counts expected at a given position of the detector due to the distribution of organ and lesion activity in the neighborhood of that position was computed. To account for the differences due to photon energy and scattering geometry, line-source response functions were measured for each possible combination of window setting, nuclide, and scattering condition. The response functions were measured to a lateral distance of 7.5 cm from the line source at which point the measured counting rate was indistinguishable from background in all cases. The Fourier transforms of these functions for various window settings are given in Figs. 1 and 2 for ^{197}Hg and ^{99m}Tc, respectively, using 7.6 cm of Lucite front-scattering material and 10 cm of backscatter material. These experimentally measured functions include the overall effects of collimator-detector efficiency, scattering, and attenuation for each window setting.

Received March 25, 1970; revision accepted April 27, 1971.

For reprints contact: A. G. Schulz, The Johns Hopkins University Applied Physics Laboratory, 8621 Georgia Ave., Silver Spring, Md. 20910.

* Present address: Div. Nuclear Medicine, Upstate Medical Center, Syracuse, N.Y.

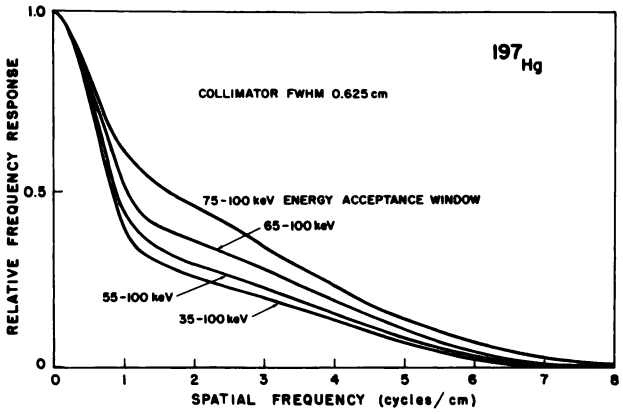

FIG. 1. Relative frequency response functions for ^{197}Hg with 10 cm of Lucite backscatter material and 7.6 cm of frontscatter material for various photon energy acceptance intervals.

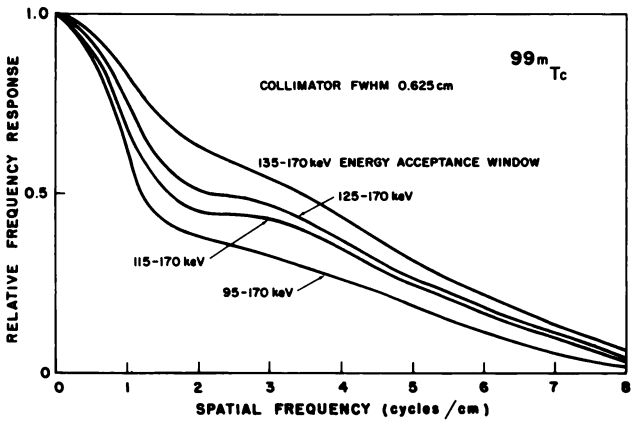

FIG. 2. Relative frequency response functions for ^{99m}Tc with 10 cm of Lucite backscatter material and 7.6 cm of frontscatter material for various photon energy acceptance intervals.

The computer program provided the interaction between the response function and the physiological target which resulted in the mathematical equivalent of scanning. A matrix of expected counts was recorded as the program scanned a rectangular pseudo-organ measuring 10 cm × 12 cm × 2.6 cm thick surrounded by tissue-equivalent scattering medium. The Fourier transforms of the response functions, Figs. 1 and 2, were combined with the spectral density functions of spheres of various sizes and then transformed to the spatial domain to generate the profile of a scanned spherical lesion. The depth of each scanned lesion profile was scaled using experimentally measured target-to-nontarget ratios for each sphere for each condition. The lesion profiles were used to generate a submatrix of mean counts which were subtracted from the mean counts due to the organ in corresponding computation cells in the program generating the display. To simulate a real scan with its associated statistical fluctuation, the average count in each cell of the "noise free" scan was replaced with an integer selected at random from a population with a Poisson distribution about the original average count. The resulting two-dimensional array of data corresponds to a scan of a cold lesion made with the detector under the specified conditions. The position of the lesion in the array was randomly varied and the data were displayed on a cathode-ray-tube display system developed for similar observer evaluation studies. The CRT measures 25.4 × 30.5 cm and provides 64 intensity levels in proportion to the count density of the simulated scan. The display is comprised of 20,000 spatial resolution cells, each measuring $\frac{1}{16} \times \frac{1}{16}$ in. A more complete description of the simulation technique and display system is contained in Refs. *3* and *4*.

LESION-DETECTION TEST PROCEDURES

Nineteen separate tests, each consisting of a sequence of 99 simulated scans, were presented to a group of five observers to establish their ability to detect the presence and location of lesions as a function of window variation.

Studies were conducted for ^{197}Hg with lesions having a diameter of 1.9 and 1.6 cm. The depth of the lesions corresponded to the position of the focal plane of the detector which was located at the center of the 2.6-cm-thick organ. For these studies, a scatter condition corresponding to 2.5 cm of scattering material above the organ was used. This corresponds to a total of 3.8 cm of scattering material above the center of the organ. A third study was also conducted for ^{197}Hg with a 1.9-cm-diam lesion and 6.3 cm of scattering material above the organ. This corresponds to a total of 7.6 cm of scattering material above the center of the lesion. For all ^{197}Hg scans, the upper energy window was set at 100 keV while the window baseline was varied from 35 to 75 keV.

A single study was conducted for ^{99m}Tc with a 1.6-cm-diam lesion and 6.3 cm of scattering material above the organ. This corresponds to a total of 7.6 cm of scattering material above the center of the lesion. The upper energy window for the ^{99m}Tc study was set at 170 keV while the window baseline was varied from 100 to 140 keV.

The observers participating in this study were engineers and physicists with several years experience with scanning instrumentation and nuclear medicine techniques. Close agreement between the detection performance of this group of observers using this display system and medically trained observers viewing normal photoscans has been established (*5*).

A typical test consisted of 106 simulated scans in which the activity level, lesion size, scatter condition, and upper energy window level were fixed,

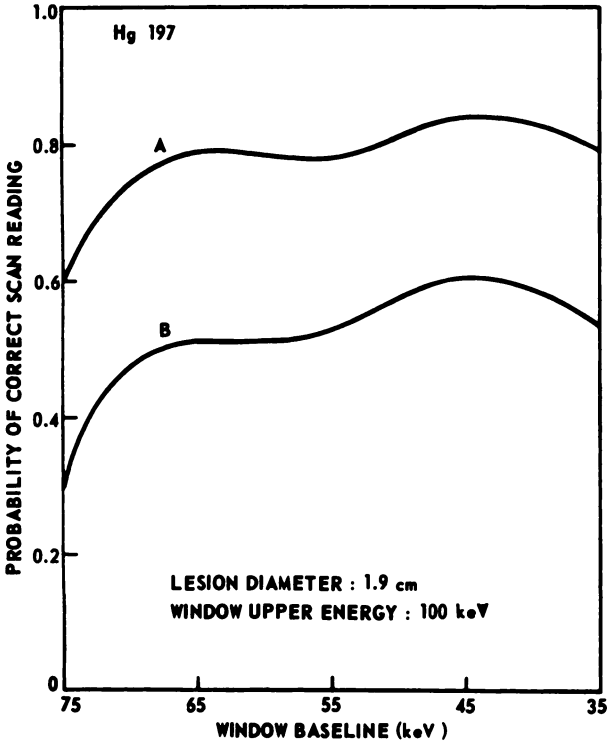

FIG. 3. Probability of correct scan reading as function of window baseline setting for 1.9-cm-diam cold lesion centered in 2.6-cm-thick slab organ beneath 2.5 cm of additional scatter material using ^{197}Hg. Curve A includes correctly assigned *no lesion, suspected lesion,* and *probable lesion* responses. Curve B includes correctly assigned *no lesion* and *probable lesion* responses.

and nine different window baseline settings were tested. The first seven scans displayed on the screen were introductory in nature while the last 99 constituted the actual test.

Two confidence levels were assigned to detections. The observer noted as *suspected lesion* those detections in which he had minimum confidence and noted as *probable lesion* those detections which appeared more certain. In tabulating these data the detection test scores are grouped into two categories. The first category includes correctly assigned *no lesion, suspected lesion,* and *probable lesion* responses. The second category includes correctly assigned *no lesion* and *probable lesion* responses. In each test approximately 20% of the scans contained no lesion. In each case the image was on the screen for 30 sec during which time the observers determined the location or absence of the lesion and recorded their observations. The same image was then shown a second time with the center of the lesion enclosed by a small box. In the absence of a lesion no indicator box appeared. Each observer indicated the correctness of his observation of a lesion at the indicated position or no lesion.

Several tests with the same simulation conditions were presented to the group to try to minimize the variation of observer performance from day to day, and the results of similar tests were combined before computing detection scores.

The parameters used in the three studies with ^{197}Hg were selected to provide a probability of detection in the range between 25% and 75%. Other studies have shown that the curves are varying rapidly in this region and changes due to varying parameters would be most obvious (*3*). The simulated activity was adjusted to give 393 counts/cm^2 with the energy window accepting photons from 65 to 100 keV. This counting rate provided a detectability in the desired range. It was elected to compare detection performance for two different lesion sizes with other conditions held constant and to compare performance for two thicknesses of frontscatter with one lesion size. When the thickness of scattering material was varied, the activity was adjusted to give equal count densities in each case for the same window setting.

RESULTS

The results of the series of tests conducted for ^{197}Hg are presented in Figs. 3–5. In each case the correct scan reading score is plotted as a function of window baseline setting for correctly assigned *no lesion, suspected lesion,* and *probable lesion* responses for one curve (Curve A); and for those correctly assigned, *no lesion,* and *probable lesion* responses for the second curve (Curve B). The tests measured the probability that the observer would correctly interpret negative scans (no lesion present)

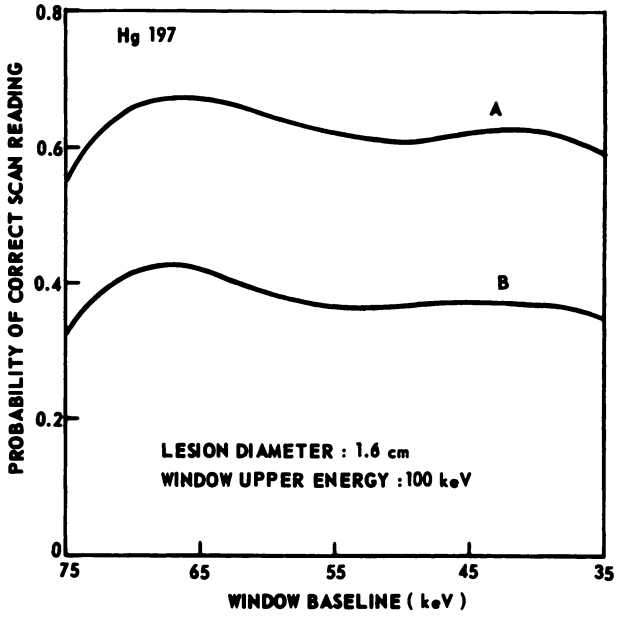

FIG. 4. Probability of correct scan reading as function of window baseline setting for 1.6-cm-diam cold lesion centered in 2.6-cm-thick slab organ beneath 2.5 cm of additional scatter material using ^{197}Hg. Curve A includes correctly assigned *no lesion, suspected lesion,* and *probable lesion* responses. Curve B includes correctly assigned *no lesion* and *probable lesion* responses.

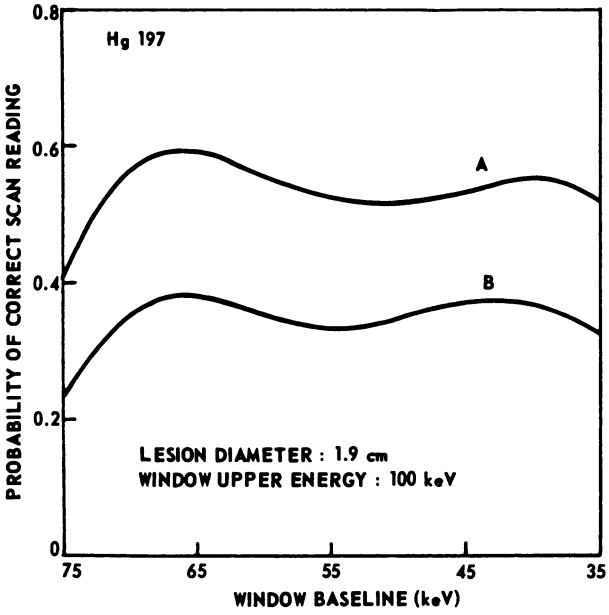

FIG. 5. Probability of correct scan reading as function of window baseline setting for 1.9-cm-diam cold lesion centered in 2.6-cm-thick slab organ beneath 6.3 cm of additional scatter material using ^{197}Hg. Curve A includes correctly assigned *no lesion, suspected lesion,* and *probable lesion* responses. Curve B includes correctly assigned *no lesion* and *probable lesion* responses.

and locate the lesion in positive scans (lesion present). In the figures it may be seen that the curves obtained for the two confidence level categories have essentially the same shape. It appears, therefore, that the factors determining the variation of detection test score are affecting both levels of confidence in the same way.

The variation of the curves with baseline window setting is unexpected. In Fig. 3 the detection test score for the 1.9-cm lesion with an effective 3.8 cm of frontscattering material is improving as the lower limit of the photon-energy acceptance window is lowered to 45 keV. This indicates that for these conditions the contribution of photons accepted in the lower energy bands enhances detectability. The signal-to-noise ratio for these photons must still be favorable to detection. The characteristics of the integrated photon counts as the window baseline energy is lowered are shown in Fig. 6. In this figure the relative count at each energy is plotted as sensitivity and is normalized to the value at 35 keV as unity. The contrast obtained with the 1.9-cm lesion at each energy is also plotted in Fig. 6. It is seen that there is no special breakpoint in these measured parameters which would explain the peak of the detectability at an integrated energy window from 45 to 100 keV shown in Fig. 3. However, ^{197}Hg photons have an associated iodine escape peak at approximately 45 keV which could contribute to the signal-to-noise ratio at this point. The contribution of these photons in enhancing detectability may be expected from the plot of the line-spread functions of the system for narrow energy windows. Shown in Fig. 7 are the line-spread functions for ^{197}Hg at the focal plane of the collimator for narrow energy windows from 40 to 45 keV, 55 to 60 keV, and 65 to 70 keV.

The line-spread function for the system with a 40–45-keV window is as sharp as that with a 65–70-keV window. The line-spread function at the intermediate energy of 55–60 keV is degraded considerably, consistent with the expectation that photons with the latter energy are almost all scattered. Below 40 keV the combined loss of contrast and the added fluctuation noise due to additional photons which are not carrying information cause the detectability to fall off.

In contrast to the results obtained with the 1.9-cm lesion, Fig. 4 shows that the optimum window for a 1.6-cm lesion has a lower energy limit of approximately 65 keV. A gradual decline in detectability is noted as the energy window baseline is lowered. The sensitivity in Fig. 6 as well as the line-spread functions in Fig. 7 all apply to this problem. The only measurement which differs for the 1.6-cm lesion is that of signal contrast which is also included in Fig. 6. For the smaller lesion the overall contrast is lower than that with the 1.9-cm diameter. The de-

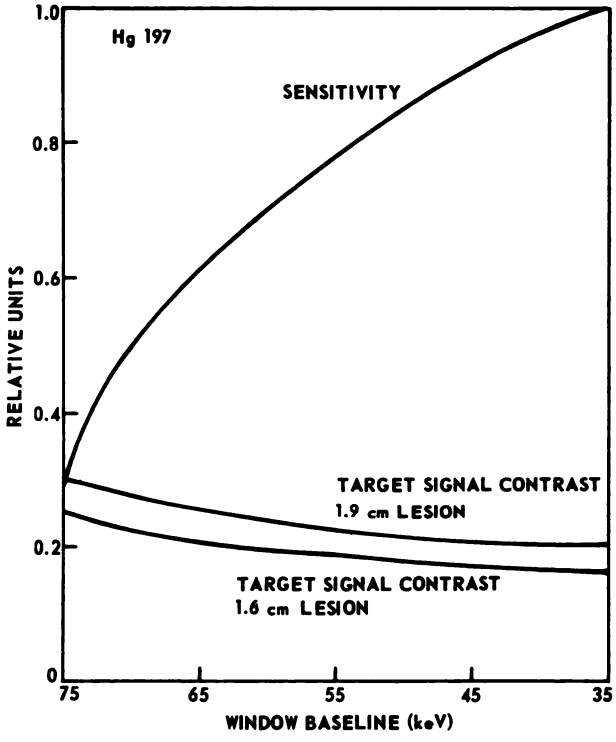

FIG. 6. Relative sensitivity and target signal contrast plotted as function of window baseline setting for ^{197}Hg. All curves relate to 2.6-cm-thick slab organ, total scatter condition of 3.8 cm measured to center of lesion, and upper energy window of 100 keV.

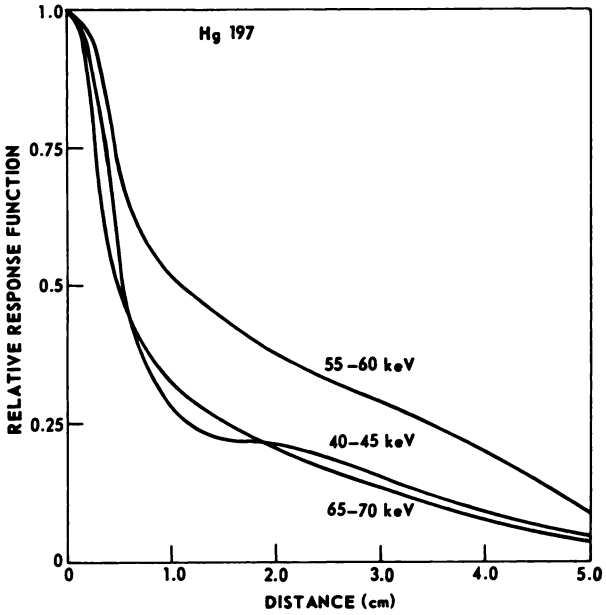

FIG. 7. Line-spread functions for ^{197}Hg for narrow energy window intervals and scatter condition of 3.8 cm.

crease in contrast at the same baseline setting is apparently below observer threshold for the noise present, and it is necessary to raise the window baseline to 65 keV to obtain best detection. On the basis of Fig. 7 it would appear that a dual-energy gate which accepted the photons around 45 keV as well as those above 65 keV would be optimum. It is interesting to note from the target signal contrast curves of Fig. 6 that the optimum position of the window baseline for each lesion size occurs where the measured contrast is approximately 0.2. The probability of reading the scan correctly with the 1.9-cm lesion when the geometry includes 7.6 cm of frontscatter material above the center of the lesion is shown in Fig. 5, plotted as a function of window baseline energy. In contrast to the performance for the same lesion size with only 3.8 cm of scattering material, the optimum window baseline is at approximately 65 keV. The shift in the optimum window baseline setting from 45 to 65 keV, when only the scatter condition is changed, can be attributed to a sharp decrease in target signal contrast caused by the inclusion of more scatter medium. Figure 5 again shows a secondary maximum in the detection at a window baseline setting of 45 keV due to the iodine escape peak.

The ability of the observer to detect lesions and correctly assess negative scans with ^{99m}Tc was determined for one scatter geometry and one lesion size. The scatter geometry consisted of backscatter plus 6.3 cm of frontscatter material above the organ (corresponding to 7.6 cm of scattering material above the center of the lesion), and the lesion diameter was 1.6 cm. The activity concentration was adjusted to give a count density of 238 counts/cm^2 for an energy window of 130–170 keV. The data plotted in Fig. 8 show that the lesion detection performance is critically dependent upon window selection. The detection score falls by almost a factor of two as the window baseline is varied by 10 keV on either side of the 130 keV optimum point. The upper curve represents detections summed over all confidence levels. The relative variation in the detection score of the lower curve is even more drastic. The rise in the detection score at the lower window baseline settings is assumed to be due to the inclusion of photons normally associated with the iodine escape peak. It is estimated from the spectra of the primary photons for this ^{99m}Tc scatter condition that approximately 10% of the photons in the primary photopeak would be added to the image data if the window baseline were lowered from 120 to 100 keV (*6*). Since spatial-resolution characteristics associated with these photons are equivalent to those of the photons in the photopeak, they tend to enhance the quality of the image. Some support for this explanation is provided by the line-spread functions corresponding to narrow energy windows plotted in Fig. 9. Experimentally-determined line-spread functions are plotted

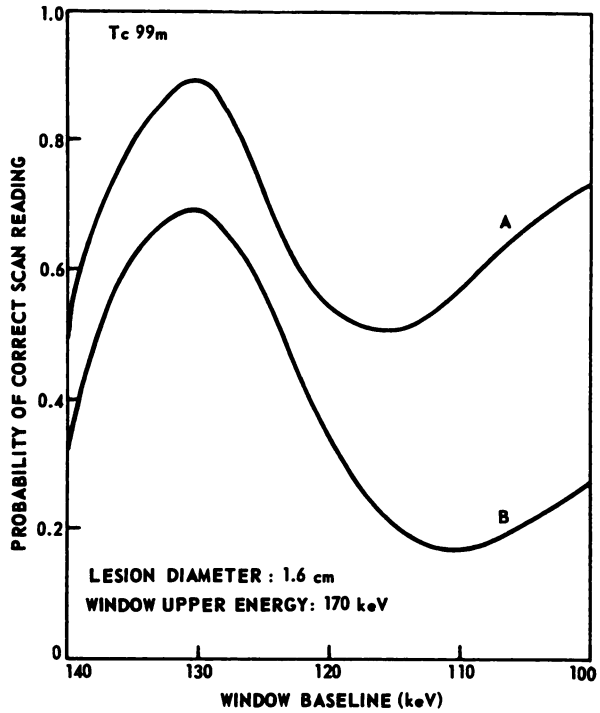

FIG. 8. Probability of correct scan reading as function of window baseline setting for 1.6-cm-diam cold lesion centered in 2.6-cm-thick slab organ beneath 6.3 cm of additional scatter material using ^{99m}Tc. Curve A includes correctly assigned *no lesion, suspected lesion,* and *probable lesion* responses. Curve B includes correctly assigned *no lesion* and *probable lesion* responses.

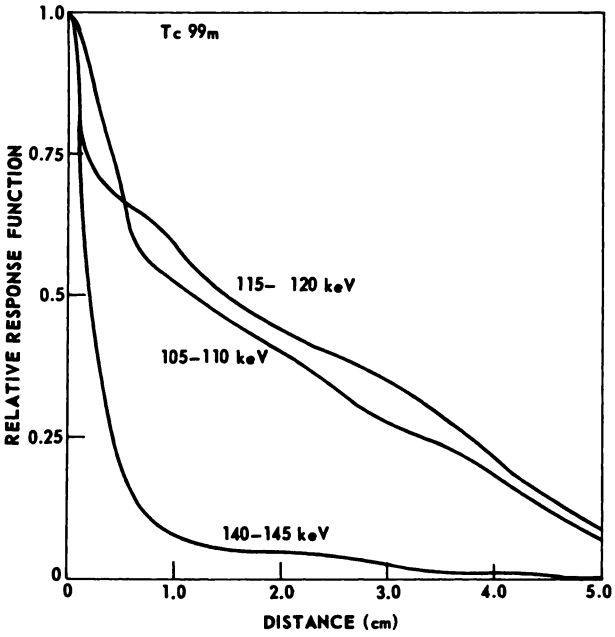

FIG. 9. Line-spread functions for ^{99m}Tc for narrow energy window intervals and frontscatter condition of 7.6 cm.

for 5-keV-wide energy windows corresponding to 140–145 keV, 115–120 keV, and 105–110 keV. It is seen that the function deteriorates from the photopeak curve at 140 keV to a curve with a very broad tail at 115–120 keV, and then sharpens up slightly as the window is lowered to 105–110 keV.

It is interesting to compare the ^{99m}Tc results in Fig. 8 with those of Fig. 5 obtained with ^{197}Hg with similar scatter conditions. It can be noted from the two curves that a 33% higher detection rate is obtained with ^{99m}Tc at its best window setting of 130–170 keV compared with ^{197}Hg at its best window setting of 65–100 keV. This occurs despite the fact that the test conditions nominally favored the ^{197}Hg. That is, the count density for ^{197}Hg was 393 counts/cm^2 while for ^{99m}Tc it was 238 counts/cm^2. In addition, the lesion sizes were 1.9 cm in the ^{197}Hg test but only 1.6 cm when ^{99m}Tc was tested. This result is in agreement with the remarkably superior target signal contrasts measured with ^{99m}Tc compared with those of ^{197}Hg (Figs. 6 and 10). In Fig. 10 the normalized sensitivity and target signal contrast are plotted as a function of energy window baseline for ^{99m}Tc. It is apparent that the improvement in detectability as the window baseline is dropped to 130 keV is due to a very sharp increase in sensitivity which overrides those losses in resolution reflected in the decreased target signal contrast ratio. As the baseline window is dropped from 125 to 115 keV, the rate of increase of sensitivity drops off slightly while the target signal contrast continues to drop sharply. This results in the indicated decrease in the observer's scan reading score. As the baseline window setting is lowered from 115 to 100 keV, the sensitivity again increases while the contrast tends to level off. This combination of events explains the observed slight increase in the probability of detection over this baseline window range.

SUMMARY

As indicated earlier, various workers have considered the effect of photon energy-window selection in scanning systems. However, systematic measurements of the effects of energy-window selection on fluctuation noise, resolution, and contrast in scan images have been lacking, and no measurements have been made of the resultant effects on observer performance in detecting lesions. In this study experimental results were used to generate simulated scans for observer tests to show how energy-window selection affects an observer's ability to detect the presence of a lesion in a scan.

The results of the observer performance studies with ^{197}Hg show peaks in the lesion-detection test scores at window baseline settings of 65 and 45 keV. The optimum value of the window baseline shifts from 65 to 45 keV as the test lesion was changed from 1.6 to 1.9 cm. The lower energy performance peak is postulated to result from the inclusion of iodine escape peak photons at the lower energy

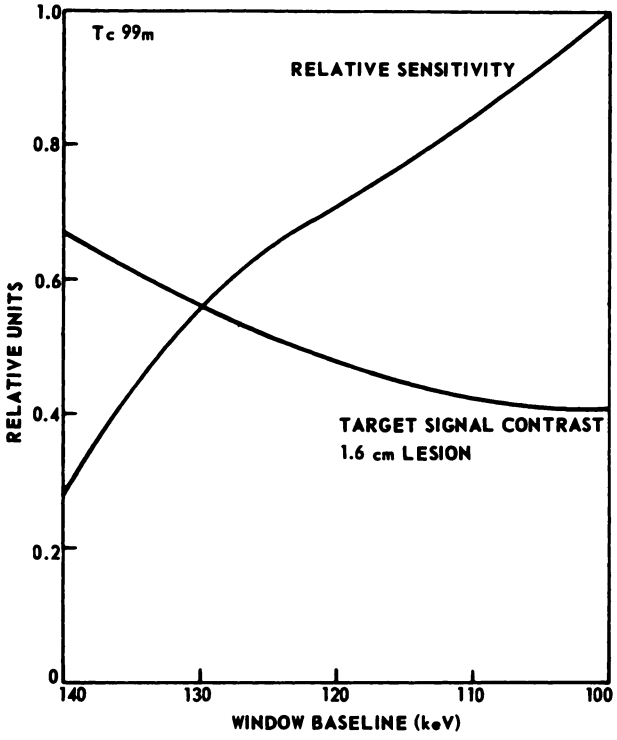

FIG. 10. Relative sensitivity and target signal contrast plotted as function of window baseline setting for ^{99m}Tc. All curves relate to 2.6-cm-thick slab organ, total scatter condition of 7.6 cm measured to center of lesion, and window upper energy of 170 keV.

window setting. Additional frontscatter material significantly reduced the overall detection rate. With additional frontscatter material the probability of correctly reading the scan has very little dependence on the window baseline setting.

The results for ^{99m}Tc showed a marked variation in detection scoring as a function of energy-window baseline setting. The observer performance peaked at a baseline setting of 130 keV and dropped by a factor of two for baseline settings only 10 keV on either side of this value. The detection performance decreases as the window baseline is lowered and then rises at a value near the iodine escape peak in a manner similar to the ^{197}Hg case. Unfortunately, the data were not taken below 100 keV. This behavior in both cases is confirmed by the narrow energy interval line-spread functions which show that the line-spread functions associated with the iodine escape peak are sharper than those appearing at intermediate energies near the photopeak.

Detectability of lesions is considerably more dependent upon window setting when using ^{99m}Tc compared with ^{197}Hg. Also, the general level of detectability is much higher for ^{99m}Tc when optimum window settings are used for both radionuclides. This observation is consistent with the superior signal contrasts measured with this nuclide compared with ^{197}Hg.

For the restricted parameters of scattering, geometry, and collimator tested, the energy-window baseline for ^{99m}Tc is critical and should be set at 130 keV for optimum performance in detecting small focal lesions.

Detection performance with ^{197}Hg does not vary greatly as the energy window is changed. The selection of a best operating point for the window baseline is not obvious. It appears that for relatively small lesions behind a thick layer of scattering medium the usual setting in the range of 60–65 keV is best. It is possible that for certain lesion and collimator combinations the 45-keV baseline setting would give better performance.

Since the "organ" used in these studies was comparable to the dimensions of the response function tails with the thicknesses of frontscattering material employed, it is expected that for larger organs the scattering effects will be slightly more pronounced. In these cases the level of detection would be slightly decreased, but the general results found above with energy-window variation would not be altered.

The rise in detectability as the energy window baseline is lowered to include the iodine escape peak indicates that a dual-energy window might provide improved performance for nuclides with primary photons in the energy range below 150 keV. The line-spread functions for narrow energy intervals showed that fewer of the photons at the iodine escape-peak energy are scattered than is the case for photons intermediate in energy between this value and the photopeak energy. The observer detection scores were consistent with these results. Therefore a dual window which accepts the photopeak and the iodine escape peak and rejects intermediate energies may give considerable performance improvement for sodium iodide detectors.

ACKNOWLEDGMENT

This work was aided by U.S. Public Health Service Grant GM 10548 and Radiological Health Training Grant 39896.

REFERENCES

1. SANDERS TP, COHEN TD, KUHL DE: Optimizing the window setting of an Anger camera for Tc-99m. *J Nucl Med* 10: 369, 1969

2. BECK RN, HARPER PV: Criteria for evaluating radioisotope imaging systems. In *Fundamental Problems in Scanning*. Springfield, Charles C Thomas, 1966

3. SCHULZ AG, KNOWLES LG, KOHLENSTEIN LC, et al: Quantitative assessment of scanning system parameters. *J Nucl Med* 11: 61–68, 1970

4. KNOWLES LG, KOHLENSTEIN LC, YATES WA: A multi-tone display for computer processed data. *J Soc Inf Display* 7: 19–22, 1970

5. KOHLENSTEIN LC, KNOWLES LG, SCHULZ AG: Comparison of the detectability of kidney lesions as a function of count density in phantom scans and computer simulated phantom scans. *J Nucl Med* 10: 415, 1969

6. ROLLO FD, SCHULZ AG: A quantitative evaluation of pulse-height selection in scanning systems. *J Nucl Med* 11: 357, 1970